Aurora A kinase inhibition destabilizes PAX3-FOXO1 and MYCN and synergizes with Navitoclax to induce Rhabdomyosarcoma cell death

Ommer, Johannes ; Selfe, Joanna L ; Wachtel, Marco ; O'Brien, Eleanor M ; Laubscher, Dominik ; Roemmele, Michaela ; Kasper, Stephanie ; Delattre, Olivier ; Surdez, Didier ; Petts, Gemma ; Kelsey, Anna ; Shipley, Janet ; Schäfer, Beat W

Abstract: The clinically aggressive alveolar rhabdomyosarcoma subtype is characterized by expression of the oncogenic fusion protein PAX3-FOXO1, which is critical for tumorigenesis and cell survival. Here we studied the mechanism of cell death induced by loss of PAX3-FOXO1 expression and identified a novel pharmacological combination therapy that interferes with PAX3-FOXO1 biology at different levels. Depletion of PAX3-FOXO1 in fusion positive (FP)-RMS cells induced intrinsic apoptosis in a NOXA-dependent manner. This was pharmacologically mimicked by the BH3 mimetic navitoclax, identified as a top compound in a screen of 208 targeted compounds. In a parallel approach, and to identify drugs that alter the stability of PAX3-FOXO1 protein, the same drug library was screened and fusion protein levels were directly measured as a read-out. This revealed that inhibition of Aurora kinase A most efficiently negatively affected PAX3-FOXO1 protein levels. Interestingly, this occurred through a novel specific phosphorylation event in and binding to the fusion protein. Aurora kinase A inhibition also destabilized MYCN, which is both a functionally important oncogene and transcriptional target of PAX3-FOXO1. Combined treatment with an Aurora kinase A inhibitor and navitoclax in FP-RMS cell lines and patient-derived xenografts synergistically induced cell death and significantly slowed tumor growth. These studies identify a novel functional interaction of Aurora kinase A with both PAX3-FOXO1 and its effector MYCN, and reveal new opportunities for targeted combination treatment of FP-RMS.

DOI: https://doi.org/10.1158/0008-5472.CAN-19-1479

Aurora A kinase inhibition destabilizes PAX3-FOXO1 and MYCN and synergizes with Navitoclax to induce Rhabdomyosarcoma cell death

Johannes Ommer[1], Joanna L. Selfe[2], Marco Wachtel[1], Eleanor M. O'Brien[2], Dominik Laubscher[1], Michaela Roemmele[1], Stephanie Kasper[1], Olivier Delattre[4], Didier Surdez[4], Gemma Petts[3], Anna Kelsey[3], Janet Shipley[2], Beat W. Schäfer[1]

[1]Department of Oncology and Children's Research Center, University Children's Hospital Zurich, Zurich, Switzerland
[2]Sarcoma Molecular Pathology Laboratory, The Institute of Cancer Research, London, SM2 5NG, UK.
[3]Department of Diagnostic Paediatric Histopathology, Royal Manchester Children's Hospital, Manchester, UK
[4] France INSERM U830, Équipe Labellisé LNCC, PSL Université, SIREDO Oncology Centre, Institut Curie, Paris, France

Running title: AURKAi and BCL-XLi synergize to control FP-RMS tumor growth

Conflict of interest: The authors declare no conflict of interest.

Corresponding author:
Beat W. Schäfer, PhD
Department of Oncology, Children's Hospital Zurich
Steinwiesstrasse 75
8032 Zurich, Switzerland
Beat.schaefer@kispi.uzh.ch
Phone: +41 (44) 266 7553
Fax: +41 (44) 266 7171

Keywords: PAX3-FOXO1, MYCN, Aurora kinase A, drug screen, BH3-mimetics, apoptosis

Word count:

Statement of significance: 17

Abstract: 248

Main text: 4558

Number of tables/figures: 6 Figures / 11 Supplemental Figures

References: 50

Abstract

The clinically aggressive alveolar rhabdomyosarcoma subtype is characterized by expression of the oncogenic fusion protein PAX3-FOXO1, which is critical for tumorigenesis and cell survival. Here we studied the mechanism of cell death induced by loss of PAX3-FOXO1 expression and identified a novel pharmacological combination therapy that interferes with PAX3-FOXO1 biology at different levels. Depletion of PAX3-FOXO1 in fusion positive (FP)-RMS cells induced intrinsic apoptosis in a NOXA-dependent manner. This was pharmacologically mimicked by the BH3 mimetic navitoclax, identified as a top compound in a screen of 208 targeted compounds. In a parallel approach, and to identify drugs that alter the stability of PAX3-FOXO1 protein, the same drug library was screened and fusion protein levels were directly measured as a read-out. This revealed that inhibition of Aurora kinase A most efficiently negatively affected PAX3-FOXO1 protein levels. Interestingly, this occurred through a novel specific phosphorylation event in and binding to the fusion protein. Aurora kinase A inhibition also destabilized MYCN, which is both a functionally important oncogene and transcriptional target of PAX3-FOXO1. Combined treatment with an Aurora kinase A inhibitor and navitoclax in FP-RMS cell lines and patient-derived xenografts synergistically induced cell death and significantly slowed tumor growth. These studies identify a novel functional interaction of Aurora kinase A with both PAX3-FOXO1 and its effector MYCN, and reveal new opportunities for targeted combination treatment of FP-RMS.

Statement of Significane

Findings show that Aurora kinase A and Bcl-2 family proteins are potential targets for fusion positive rhabdomyosarcoma.

Introduction

Rhabdomyosarcomas (RMS) are the most common pediatric soft tissue sarcoma. The most aggressive subtype, alveolar Rhabdomyosarcoma, is characterized by the occurrence of balanced reciprocal translocations resulting in expression of oncogenic fusion proteins (1,2), whereby the most common fusion is PAX3-FOXO1. Fusion-positive RMS (FP-RMS) has a high propensity to metastasize and resistance to standard-of-care treatments are common, resulting in 5-year survival rates of only about 30% (3-5). The search for novel targeting strategies is difficult as pediatric tumors generally harbor only few somatic mutations (6), which is especially true for the FP-RMS subtype (7). The lack of other somatic mutations underscores the important role of PAX3-FOXO1, which functions as transcriptional activator affecting multiple oncogenic pathways (8). We previously demonstrated that antisense-mediated loss of PAX3-FOXO1 results in cell death, underscoring the addiction of FP-RMS cells to the fusion protein. However, so far the exact mechanism by which the cells die has not been described (9).

Due to its importance for tumor cell survival, therapeutic targeting of PAX3-FOXO1 has become a paramount goal of rhabdomyosarcoma research. One approach has been to identify key downstream effectors of the fusion protein as potential therapeutic targets, such as MYCN (10). However, since MYCN and PAX3-FOXO1 are transcription factors lacking enzymatic activity, targeting these proteins directly is challenging. Recently, new strategies have been developed targeting PAX3-FOXO1 indirectly by inhibiting its stabilizer Polo-like kinase 1 (PLK1) (11) or its co-factors, like bromodomain-containing protein 4 (BRD4) (12) or chromodomain-helicase DNA-binding protein 4 (CHD4) (13). Further strategies to target PAX3-FOXO1 and MYCN are reviewed in (14,15). While single-target therapies can be efficient in pre-clinical models and clinical treatment, they are prone to develop therapy resistance. One way to circumvent this problem is to use drug combinations that target different pathways preventing escape.

Recently, we showed that PLK1 stabilizes PAX3-FOXO1 through phosphorylation of serines 503 and 505, protecting the fusion protein from proteasomal degradation (11). While single-agent inhibition of PLK1 proved very effective in reducing tumor growth in vivo, resistance against this treatment was also observed. One of the regulators of PLK1 is Aurora A kinase (AURKA) which therefore might also functionally contribute to FP-RMS tumorigenesis. Aurora kinases are a family of serine-threonine kinases that are involved in cell cycle progression, most importantly during mitosis (16). AURKA is highest expressed at the G2/M transition (17) where it activates PLK1 by phosphorylation at threonine 210 as crucial step for checkpoint recovery (18,19). Furthermore, AURKA serves important roles in centrosome maturation and mitotic entry (20), as well as for spindle assembly (21). These

functions in cell cycle progression indicate an important role for Aurora kinases in cancer. Indeed, AURKA is upregulated in a variety of tumors and has thus become a focus of inhibitor development (22-25). AURKA has also been shown to phosphorylate AKT and mTOR indicating a role in promoting chemotherapy resistance (26).

Our goal was thus to find a novel synergistic combination therapy to treat FP-RMS. We demonstrate that FP-RMS cells undergo intrinsic apoptosis in a NOXA-dependent manner after loss of PAX3-FOXO1 which can be enhanced by the BH3-mimetic navitoclax (ABT-263). Moreover, we established a novel functional link between AURKA and stability of both PAX3-FOXO1 and MYCN. Combination of navitoclax and alisertib had synergistic anti-tumor effects *in vitro* and *in vivo* and thus provides the basis for a promising new rationale combination therapeutic approach for FP-RMS.

Material and Methods

Cell lines

Rhabdomyosarcoma cell lines RD, Rh4 (Peter Houghton, St. Jude Children's Hospital, Memphis, TN), RhJT (Scott Diede, Fred Hutchinson Cancer Research Center, Seattle, WA), RMS (Janet Shipley, Sarcoma Molecular Pathology, The Institute of Cancer Research, London, UK), KFR (Jindrich Cinatl, Frankfurter Stiftung für krebskranke Kinder, Frankfurt, Germany), Rh30 as well as HEK293T cells (both ATCC LGC Promochem) were cultured in high glucose DMEM (Sigma-Aldrich), supplemented with 100 U/mL penicillin/streptomycin, 2 mmol/L L-glutamine, and 10% FBS (Life Technologies) at 37°C and 5% CO_2. All RMS cell lines were authenticated upon receipt by short tandem repeat (STR) profiling, and used for experimentation from frozen stocks within 10-20 further passages. As the human myoblast cell line has not yet been characterized by STR profiling, negative matching with all available cell lines in the database was used for verification. All cells were regularly tested for mycoplasma contamination by a PCR based assay.

Cells from patient-derived xenografts (PDX)

PDX tumors were dissociated as described before (27). In brief, tumor tissue was minced with scalpels and suspended in Hanks' Balanced Salt Solution (HBSS, Sigma-Aldrich) supplemented with 1 mmol/L $MgCl_2$, 200 μg/mL Liberase, and 200 U/mL DNase I (both Roche). Tissue was digested for 30 minutes

at 37°C and filtered twice through 70 μm cell strainers (BD Biosciences). Dissociated cells were washed with phosphate-buffered saline (PBS, Sigma-Aldrich) before freezing or resuspending for further culture. Cells derived from PDX tumors were cultured in Neurobasal medium (Life Technologies) supplemented with 2x B-27™ Supplement (Life Technologies), 20 ng/mL EGF and 20 ng/mL basic FGF (Peprotech) on plates coated with Matrigel® (Corning Life Sciences).

In vitro drugs screenings

Cells were seeded in 384-well plates and shRNA was induced by 100 ng/ml doxycycline (Sigma-Aldrich). Drugs (Supplemental Table 1) were purchased from Selleckchem and added to the cells using the HP D300 Digital Dispenser (Tecan). 24h after seeding cells, medium was changed to 19 μl culture medium. Drugs were pre-diluted to 10 μmol/l in culture medium and 1 μl of each drug was added to the wells for a final concentration of 500 nmol/l. Viability was measured after 48h by WST-1 assay.
Cells for immunoblot analysis were seeded in 24-well plates and drugs added at 100 nmol/l after 48h of incubation.

Mouse xenograft experiments

NOD/Scid il2rg$^{-/-}$ (NSG) mice were 8-12 weeks old for the experiments. 5x10^6 Rh4 or IC_PPDX35 cells were injected subcutaneously into the flanks. After engraftment mice were randomized into 4 groups (5-6 mice per group) when tumors reached 100 mm^3. Tumor growth was assessed by caliper measurements and the volumes were calculated using the formula V= (4/3) π r3; r=(d1+d2)/4). Mice were sacrificed when the tumor volume reached 1000 mm^3. All animal experiments have been approved by the Swiss veterinary authorities (license ZH206/15).

Statistics

Data analysis was performed with GraphPad Prism 7. Significance was calculated using unpaired two-tailed Student's t-test or Welch's two-tailed test. Two-way ANOVA was used for multiple comparisons. Differences were considered statistically significant with $p<0.05$. Drug synergy was calculated using the Bliss independence model in the free SynergyFinder WebApp (28).

Additional methods see supplemental material and methods section.

Results

Silencing of PAX3-FOXO1 expression induces intrinsic apoptosis in a NOXA-dependent manner

Since it was previously shown that silencing of PAX3-FOXO1 expression results in FP-RMS cell death (9), we aimed first to further elucidate its precise mechanism.

We generated FP-RMS cell lines expressing an inducible shRNA (shP3F) or control (shsc) to specifically silence PAX3-FOXO1 expression upon doxycycline treatment (Suppl.Fig.1A). After confirming that the system significantly downregulated the fusion protein both at the mRNA and protein level in four different cell lines (Suppl.Fig.1B-D), we assessed whether cells would undergo apoptosis. We observed a significant increase in caspase 3/7 activity in Rh4 and Rh30 cells after P3F depletion compared to control (Fig.1A, Suppl.Fig.1E). This increase was also reflected by the appearance of cleaved products of PARP, caspases 3, 7, and 9 (Fig.1B). To exclude off-target effects, we overexpressed a non-targetable PAX3-FOXO1 mutant which indeed could rescue cells from apoptosis despite silencing of the endogenous fusion protein as shown by reduced caspase 3/7 activity (Suppl. Fig1F) and decreased levels of cleaved PARP and caspase 3 protein products (Suppl. Fig.1G).

To further confirm this notion, we also treated cells after fusion protein depletion with increasing concentrations of the pan-caspase inhibitor zvad-FMK which again could restore viability of shP3F-Rh4 cells (Fig.1C) and reduced cleaved PARP and caspase 3 protein levels (Suppl.Fig.1H). To exclude other modes of cell death, we also treated cells with the different cell death inhibitors zvad-FMK (apoptosis) necrostatin-1 (necroptosis), ferrostatin (ferroptosis), as well as E64d (cathepsin inhibitor) and cathepsin GI. However, only zvad-FMK could rescue viability but none of the other inhibitors (Fig.1D). These data indicate that apoptosis is the major mode of cell death activated in FP-RMS cells upon depletion of PAX3-FOXO1.

Next, we sought to identify the pro-apoptotic protein(s) responsible for initiating apoptotic cell death. We performed a small scale CRISPR/Cas9 screen in shP3F-Rh4 cells using the construct depicted in Suppl.Fig.2A to knock-out pro-apoptotic genes either individually or in combination, and measured cell viability upon P3F depletion. Knock-down efficiencies of Bax, Bak, Bad, Bim as examples are shown in Suppl.Fig.2B-C. In control cells (shsc-Rh4), only depletion of caspase 9, but not caspase 8, and the combination of Bax/Bak were able to significantly reduce caspase 3/7 activity (Suppl.Fig.2D). This indicates that activation of the extrinsic pathway is less important in FP-RMS cells. Upon depletion of PAX3-FOXO1, NOXA was the only BH3-only protein capable to significantly reduce caspase 3/7 activity (Fig.1E, Suppl.Fig.2E), similar to knock out of the pore forming proteins BAX and BAK. These

results were validated in three additional FP-RMS cell lines (Suppl.Fig.2F), albeit the extent of repression differed among cell lines. Nevertheless, NOXA seems to play an important role in initiating apoptosis after PAX3-FOXO1 depletion, although the contribution of other BH3-only proteins cannot be excluded. Furthermore, cell cycle analysis after PAX3-FOXO1 silencing (shP3FDox) indicated no significant change in cell cycle distribution but appearance of a sub-G1 peak in all cells except Rh30, indicative of induction of apoptosis (Suppl.Fig.2G). This is in line with the observation that both NOXA mRNA and protein expression are upregulated upon silencing of the fusion protein in all cell lines tested with the exception of Rh30 cells (Fig.1F-G, Suppl.Fig.2H). Taken together, our results demonstrate that intrinsic apoptosis initiated upon silencing of PAX3-FOXO1 depends on upregulation of the BH3-only protein NOXA.

The BH3-mimetic navitoclax enhances cell death after PAX3-FOXO1 depletion

Next, we aimed to find drugs that would enhance apoptosis induced by PAX3-FOXO1 depletion. For this, we set up a compound screen of 208 drugs at a final concentration of 500nM and treated shP3F-Rh4 cells after doxycycline-mediated shRNA induction (Suppl.Fig.3A, Suppl. Table 1). Results are depicted as ratio of viability comparing shP3F versus shsc cells. The screen identified 13 candidate drugs that decreased viability by at least an additional 50% while remaining unchanged in control cells (Fig.2A, left panel; raw data Suppl. Table 2). Classification of the top hits according to their mechanism of action revealed that three of them are BH3-mimetics (Fig.2A, right panel) with navitoclax (ABT-263) being the most potent drug, also when validating each as single agent (Fig.2B, Suppl.Fig.3 B-M). To directly compared BCL-XL versus BCL-2 targeting, we generated dose-response curves for navitoclax and venetoclax (ABT-199) (Fig.2C-D). Interestingly, navitoclax reduced IC_{50} to at least a ten times lower concentration (reduction of 3.0μM to 0.18μM) than venetoclax (reduction of 9.6uM to 5.6uM). These findings suggest that inhibition of BCL-2 might be less important. To confirm this notion, we treated cells with increasing concentrations of an additional BCL-X_L specific inhibitor, A1331852, and UMI-77 which is MCL-1 specific. While A1331852 showed comparable effects to navitoclax (Fig.2E), treatment with UMI-77 did not further increase cell death (Suppl.Fig.3N). These results strengthen the observation that PAX3-FOXO1 silencing primes FP-RMS cells to apoptosis via balancing NOXA versus BCL-XL levels.

To demonstrate this more directly, we treated shP3F-Rh4-NOXA$^{-/-}$ cells (Suppl.Fig.2E) with navitoclax and found indeed reduced sensitivity upon silencing of PAX3-FOXO1 (Fig.2F). Finally, expression analysis of different datasets in the r^2 database (R2: Genomics Analysis and Visualization

Platform: *http://r2.amc.nl*) revealed that NOXA expression was elevated at base levels in all rhabdomyosarcoma datasets compared to healthy skeletal muscle tissue (Suppl.Fig.3O).

These findings suggest that rhabdomyosarcoma cells might be already primed towards a pro-apoptotic state through higher basal NOXA expression which can be further enhanced by reduction of fusion protein levels and renders them more sensitive towards navitoclax treatment.

Aurora kinase A inhibition reduces PAX3-FOXO1 protein stability

Next, we aimed to pharmacologically reduce PAX3-FOXO1 protein levels. To this end, we treated wild type Rh4 cells with the same drug library (Supplemental Table 1) and analyzed cell lysates by Western Blot (Suppl.Fig.4A). To exclude general toxic effects all signals were densitometrically digitalized and normalized to the house keeping protein GAPDH. Initial hits were called when fusion protein levels were lowered below 80%, a criterion fulfilled by 43 compounds (Fig.3A-B; raw data Suppl. Table 3). When classifying these hits according to their drug targets, we identified five epigenetic regulators, though HDAC inhibitors like entinostat, which was recently described to reduce fusion protein levels (29), showed only mild to no effects (Suppl. Fig 4B). Furthermore, we classified five proteasome, five AURKA, and three CDK9 inhibitors (Fig.3C). Strikingly, AURKA inhibitors were already identified in our apoptosis screen as hits (Fig. 2B), and previous work from our laboratory demonstrated a direct interaction between PAX3-FOXO1 and Polo-like kinase 1 (PLK1) which stabilizes the fusion protein (11) and is known to be activated by AURKA (19). Hence, we individually validated AURKA inhibitors at increasing doses and identified alisertib as being the compound active at the lowest doses tested (Fig.3D, Suppl.Fig.4C-D). Importantly, treatment of PDX-derived primary cells with alisertib also reduced fusion protein levels (Suppl.Fig.4D). We were then interested to study the mechanism underlying the functional interaction of AURKA and PAX3-FOXO1. We treated Rh4 cells with alisertib which increased total protein levels of both PLK1 and AURKA, whereas we observed a reduction of PLK1 phosphorylation at threonine 210, as expected (Fig.3E). Since AURKA has been described to phosphorylate S256 in wild type FOXO1 (30), we then investigated phosphorylation of S437 in PAX3-FOXO1 (corresponding residue in wild-type FOXO1). Indeed, we also observed a clear reduction at this site upon alisertib treatment (Fig.3E). As this region of PAX3-FOXO1 has been described to be relevant for protein stability (reviewed in (15)), we next studied whether phosphorylation of S437 contributed to fusion protein stability by replacing serine with alanine. Interestingly, and actually even slightly more pronounced than

the previously described S503A mutant, the S437A mutant also significantly reduced fusion protein stability as revealed after 8hr treatment with cycloheximide (Fig.3F-G).

Lastly, to investigate a potential direct interaction of AURKA and PAX3-FOXO1 we fused PAX3-FOXO1 to the bacterial biotin-ligase BirA (31) and expressed it ectopically in HEK293T cells. After pull down of biotinylated proteins using streptavidin coated beads, PLK1 was identified on Western Blots in fusion protein samples but not in the BirA-only control, as shown before (32) (Fig.3H). Strikingly, also AURKA was identified in this assay as being selectively biotinylated, suggesting a novel direct interaction of this kinase and the fusion protein (Fig.3H).

Taken together, our results indicate that AURKA inhibition can decrease fusion protein stability through reduced phosphorylation of serine 437 which might contribute to its ability to induce apoptosis in FP-RMS cells.

Aurora kinase A inhibition also destabilizes MYCN in FP-RMS cell lines

AURKA is reported to stabilize the MYCN protein that is highly expressed through transcriptional regulation by the fusion protein and genomic amplification (10,33-35). Previous studies showed that AURKA stabilizes MYCN by interfering with SCF^{FbxW7}-mediated ubiquitination and that sequential phosphorylation of MYC proteins at S62 and T58 is required for binding of SCF^{FbxW7} (36,37). We therefore investigated whether AURKA inhibition affected MYCN protein levels in FP-RMS cells. We stably transduced three different FP-RMS cell lines with plasmids expressing shRNA against AURKA mRNA. In all cell lines depletion of AURKA resulted in reduced MYCN protein levels (Fig.4A). In accordance with published literature (38), MYCN double-mutants (T58A / S62A) had more stable MYCN and were rescued from degradation after depletion of AURKA in RMS cells (Fig.4B). This finding indicates that in FP-RMS cells MYCN stability is controlled by AURKA through the same mechanisms described for other cell types and cancers (39). Lastly, we wanted to confirm the influence of pharmacological AURKA inhibition on MYCN protein levels in FP-RMS cells. We treated different FP-RMS cell lines with increasing concentrations of the AURKA inhibitors alisertib, as well as CCT137690 (a kinase inhibitor), and CD532 (an amphosteric inhibitor with similarities to alisertib), respectively. In all cell lines, inhibition of AURKA resulted in loss of MYCN protein levels in a dose dependent manner at sub-micromolar doses (Fig.4C, Supp. Fig.5A-B).

Taken together, our data shows that AURKA stabilizes MYCN in addition to its effects on PAX3-FOXO1 and its inhibition destabilizes MYCN, a target gene of the fusion protein.

Alisertib and navitoclax act synergistically in vitro

Since it is unlikely that single agents will be able to provide significant clinical benefit, we next wanted to identify a combination of synergistically acting drugs. To do this in an unbiased way, we screened our library for compounds that would synergistically reduce cell viability in conjunction with a non-effective concentration of navitoclax (IC_{20}) (Suppl.Fig.6A-B; raw data Suppl. Table 4). We assessed cell viability after 48h and ranked the results according to synergism. Strikingly, out of the 28 hits identified, seven were AURKA inhibitors (Fig.5A). Six of these were also identified in a similar screen carried out in a second FP-RMS cell line (Suppl.Fig.6C-D). Hence, AURKA inhibitors might act in synergy with navitoclax. To test this, we treated FP-RMS cells with increasing concentrations of both alisertib and navitoclax to obtain a combination matrix. Indeed, the combination was able to induce cell death even at lower drug concentrations (Fig.5B) and was highly synergistic as assessed by SynergyFinder (28) (Fig.5C, Suppl.Fig7A). Importantly, we observed comparable synergistic effects not only in cell lines but also in six PDX-derived primary cells. This synergy was tumor specific as non-tumorigenic cells (human foreskin fibroblasts and myoblasts) were not sensitive towards the combination treatment despite expression of various levels of NOXA (Suppl.Fig.7B). $NOXA^{-/-}$ cells were also not sensitive to the combination treatment, demonstrating that NOXA expression was required (Suppl.Fig.8A-B).

As AURKA plays an important role for cell cycle progression during G_2/M phase, we assessed cell cycle distribution after alisertib or combination treatment. Treating cells with 50 or 100 nM alisertib, we observed an increasing proportion of cells arrested in G_2/M phase (Fig.5D). Combination with 800nM navitoclax however strongly reduced the G_2/M peak and increased the sub-G_1 fraction (Fig.5D, Suppl.Fig.8C). This suggests that alisertib alone induces cell cycle arrest while in combination with navitoclax pushes cells into apoptosis. These findings are also supported by a synergistic increase in caspase 3/7 activity (Suppl.Fig.8D). Hence, alisertib acts synergistically with navitoclax *in vitro* to induce apoptosis in cell lines and primary PDX-derived RMS cells, while the drug combination had no major effects on non-tumorigenic cells.

Combination of alisertib and navitoclax synergistically reduces tumor growth in vivo

Having confirmed a synergistic action of alisertib and navitoclax in vitro, we next aimed to assess the anti-tumorigenic response of the combination in vivo. We injected NOD/Scid $il2rg^{-/-}$ (NSG) mice subcutaneously with either Rh4 or patient-derived IC_pPDX35 cells. After tumors were palpable, mice

were randomized into four groups and treated daily over three weeks with either vehicle, navitoclax alone (80 mg/kg), alisertib alone (30 mg/kg), or the combination of both drugs (Suppl.Fig.9A). While continuous tumor growth was observed in Rh4 cells in vehicle and navitoclax only treated mice, alisertib treatment slightly delayed tumor growth but failed to induce lasting effects (Fig.6A). In contrast, combination therapy resulted in modest tumor regression and lasting stable disease even after end of the treatment period (Fig.6A). This was also reflected in the survival of mice, since only animals in the combination group survived (Fig.6B). In the PDX model, alisertib treatment alone provoked a stronger delay in tumor growth albeit also in this setting, combination treatment showed the most stable growth control (Fig.6C) and survival was increased (Fig.6D). In neither experiment, we observed significant weight loss (Suppl.Fig.9B-C). To investigate whether alisertib treatment mimics PAX3-FOXO1 depletion, we also performed an in vivo experiment with the doxycycline inducible shP3F line in combination with navitoclax. While silencing of the fusion protein alone already leads to significant growth inhibition, addition of navitoclax treatment has a further, albeit small, combinatorial effect (Suppl. Fig. 9D). We also isolated IC_pPDX35 tumors after one week of treatment, where histological analysis revealed a marked increase in the number of apoptotic cells in combination treated tumors (Fig.6E) and increased staining for cleaved caspase 3 (Fig.6E). Consequently, proliferation was reduced as monitored by Ki67 staining and increased expression of p21 (Suppl.Fig.9E,F).

To underscore the clinical relevance of AURKA inhibition, we finally noticed that AURKA RNA expression is significantly higher in three independent rhabdomyosarcoma datasets compared to healthy skeletal muscle (Fig.6F) (data from R2 database: *http://r2.amc.nl*). Further, we demonstrated AURKA protein expression in the majority of primary RMS. 26/37 (70%) of FP-RMS and 37/44 (84%) of FN-RMS stained positively for AURKA by IHC (Suppl.Fig.10A-B). In addition, AURKA and the proliferation marker Ki-67 showed a significant correlation in FN-RMS and a trend toward significance in FP-RMS (Suppl.Fig.10C-D). This was consistent with significant correlations between *AURKA* and *MKI67* at the mRNA level (Suppl.Fig.10E-F). No significant correlations between AURKA immunohistochemistry (IHC) scores and event or overall survival were seen in either the FP or FN groups.

Discussion

Our aim for this study was to identify a novel synergistic combination treatment strategy based on cell death mechanisms identified in FP-RMS following silencing of PAX3-FOXO1. We showed that cells undergo intrinsic apoptosis in a NOXA-dependent manner upon reduction of PAX3-FOXO1 protein levels. In accordance, we identified BH3-mimetics, specifically navitoclax, to efficiently enhance this mode of cell death. Furthermore, we demonstrated a novel functional interaction between AURKA and the fusion protein and observed strong synergy in vitro and in vivo with the AURKA inhibitor alisertib and navitoclax.

We established a functional link between PAX3-FOXO1 and the BH3-only protein NOXA. However, we were unable to identify exactly how the fusion protein regulates NOXA expression. Previously, it was reported that PAX3-FOXO1 can upregulate basal Noxa levels in mouse myoblasts which could prime tumor cells to apoptosis (40). Indeed, we also found that NOXA levels in tumor cells are higher than in normal myoblasts. However, in ChIPseq data, we could not detect any binding of PAX3-FOXO1 to the genomic NOXA locus (41), excluding a direct role of the fusion protein in NOXA regulation. This is supported by the observation that NOXA levels even further increase when PAX3-FOXO1 levels diminish. Since the cell lines used in our experiments are p53 deficient (42), this also excludes a role of p53 in NOXA regulation as previously described (43). However, it is well known that NOXA gene expression can be induced by a variety of cellular stresses such as hypoxia, DNA damage, genotoxic, ER or metabolic stress (44). If any of these and which one might be responsible for the observed phenotype remains to be investigated.

Nevertheless, the observation that NOXA upregulation was required for apoptosis of FP-RMS cells led to the identification of navitoclax as sensitizer. This is in line with the previous identification of the BCL-XL inhibitor A-1331852 as sensitizer to chemotherapeutics (45). In addition, BCL-XL has been described as target gene of the fusion protein (46), which also explains the lower sensitivity of FP-RMS cells to venetoclax, targeting BCL-2. However, single agent activity is likely limited and therefore we searched for drugs capable to reduce fusion protein levels using conventional western blotting. This led to the identification of multiple AURKA inhibitors that also reduced MYCN protein levels, a functionally very important PAX3-FOXO1 target gene (35).

Previously it was reported that fusion protein levels could be reduced by entinostat, an HDAC inhibitor (29). Conversely, in our screen for drugs affecting fusion protein levels, epigenetic regulators, like entinostat or SAHA do not show a striking effect. However, the drug concentrations used in our

screen, as well as incubation times (0.1 µM for 48h) are substantially lower than what was used by Abraham and colleagues (2 µM for 72h) (29). It is possible that these factors are the reasons for epigenetic regulators like entinostat not showing strong effects in our screen (Suppl. Fig. 3B).

Strikingly, we identified a new phosphorylation site in PAX3-FOXO1 (serine 437) that is important for fusion protein stability. This site corresponds to S256 in wild-type FOXO1, where it regulates nuclear exclusion and subsequent degradation (47) whereas phosphorylation of S437 in PAX3-FOXO1 stabilizes the fusion protein. These seemingly opposing effects on protein stability might suggest that protein turnover of wt versus the fusion protein are regulated by different mechanisms, as recently also suggested for the EWS-FLI1 fusion expressed in Ewing sarcoma (48). A similar observation has already been described for acetylation of K426 and K429 by the histone actyltransferase KAT2B that also stabilize PAX3-FOXO1 (49). Acetylation of the corresponding sites in wild-type FOXO1 results in phosphorylation at S256 and subsequent degradation (27). Hence, we might speculate that acetylated K426/K429 might contribute to stability through priming of the fusion protein for S437 phosphorylation.

In the past, clinical trials involving navitoclax or alisertib have been challenging halting the process of clinical development. Navitoclax is known to increase the risk for thrombocytopenia due to its on-target effect (50). The advantage of our synergistic combination approach is that the individual drug doses can be lowered, thereby potentially reducing unwanted effects of each individual drug. Indeed, in our in vivo experiments we did not observe complications when using both drugs in combination. Furthermore, recent interest in these drugs increased and both companies are currently recruiting to new clinical trials (www.clinicaltrials.gov).

Taken together, we identified a previously undescribed site in PAX3-FOXO1 that is important for fusion protein stability. With AURKA inhibition, we found a therapeutic option to target this site in the fusion protein while simultaneously also affecting MYCN levels (Suppl.Fig.11A-B). It is likely that both fusion protein and MYCN levels contribute to the inhibitory effects of alisertib since positive feedback mechanisms have been described regulating the expression of these two proteins [10, 12]. Furthermore, by characterizing the exact mechanism of cell death associated with loss of fusion gene expression we were able to identify drugs that enhance this mode of cell death. When used in such a rationale combination, both drugs show a high degree of synergy both in vitro and in vivo, in cell lines and a RMS PDX model. These findings shed more light on a devastating disease and may offer novel therapeutic options for the treatment of patients with alveolar rhabdomyosarcoma.

Acknowledgments

The authors wish to acknowledge the financial support from Swiss National Science Foundation (310030_156923 and 31003A_175558), Childhood Cancer Research Foundation Switzerland, and Cancer League Switzerland (KLS-3868-02-2016).

References

1. Barr FG, Biegel JA, Sellinger B, Womer RB, Emanuel BS. Molecular and cytogenetic analysis of chromosomal arms 2q and 13q in alveolar rhabdomyosarcoma. Genes, chromosomes & cancer 1991;3(2):153–61.
2. Barr FG, Holick J, Nycum L, Biegel JA, Emanuel BS. Localization of the t(2;13) breakpoint of alveolar rhabdomyosarcoma on a physical map of chromosome 2. Genomics 1992;13(4):1150-6.
3. Breneman JC, Lyden E, Pappo AS, Link MP, Anderson JR, Parham DM, et al. Prognostic Factors and Clinical Outcomes in Children and Adolescents With Metastatic Rhabdomyosarcoma—A Report From the Intergroup Rhabdomyosarcoma Study IV. Journal of Clinical Oncology 2003;21(1):78–84.
4. Missiaglia E, Williamson D, Chisholm J, Wirapati P, Pierron G, Petel F, et al. PAX3/FOXO1 fusion gene status is the key prognostic molecular marker in rhabdomyosarcoma and significantly improves current risk stratification. Journal of clinical oncology : official journal of the American Society of Clinical Oncology 2012;30(14):1670–77.
5. Williamson D, Missiaglia E, Reyniès A, Pierron G, Thuille B, Palenzuela G, et al. Fusion gene-negative alveolar rhabdomyosarcoma is clinically and molecularly indistinguishable from embryonal rhabdomyosarcoma. Journal of clinical oncology : official journal of the American Society of Clinical Oncology 2010;28(13):2151–58.
6. Vogelstein B, Papadopoulos N, Velculescu VE, Zhou S, Diaz LA, Kinzler KW. Cancer genome landscapes. Science (New York, NY) 2013;339(6127):1546–58.
7. Shern JF, Chen L, Chmielecki J, Wei JS, Patidar R, Rosenberg M, et al. Comprehensive genomic analysis of rhabdomyosarcoma reveals a landscape of alterations affecting a common genetic axis in fusion-positive and fusion-negative tumors. Cancer discovery 2014;4(2):216–31.
8. Fredericks WJ, Galili N, Mukhopadhyay S, Rovera G, Bennicelli J, Barr FG, et al. The PAX3-FKHR fusion protein created by the t(2;13) translocation in alveolar rhabdomyosarcomas is a more potent transcriptional activator than PAX3. Molecular and cellular biology 1995;15(3):1522–35.
9. Bernasconi M, Remppis A, Fredericks WJ, Rauscher FJ, Schäfer BW. Induction of apoptosis in rhabdomyosarcoma cells through down-regulation of PAX proteins. Proceedings of the National Academy of Sciences of the United States of America 1996;93(23):13164–69.
10. Tonelli R, McIntyre A, Camerin C, Walters ZS, Di Leo K, Selfe J, et al. Antitumor activity of sustained N-myc reduction in rhabdomyosarcomas and transcriptional block by antigene therapy. Clinical cancer research : an official journal of the American Association for Cancer Research 2012;18(3):796–807.
11. Thalhammer V, Lopez-Garcia LA, Herrero-Martin D, Hecker R, Laubscher D, Gierisch ME, et al. PLK1 phosphorylates PAX3-FOXO1, the inhibition of which triggers regression of alveolar Rhabdomyosarcoma. Cancer research 2015;75(1):98–110.

12. Gryder BE, Yohe ME, Chou H-C, Zhang X, Marques J, Wachtel M, et al. PAX3-FOXO1 Establishes Myogenic Super Enhancers and Confers BET Bromodomain Vulnerability. Cancer discovery 2017;7(8):884–99.
13. Böhm M, Wachtel M, Marques JG, Streiff N, Laubscher D, Nanni P, et al. Helicase CHD4 is an epigenetic coregulator of PAX3-FOXO1 in alveolar rhabdomyosarcoma. Journal of Clinical Investigation 2016;126(11):4237–49.
14. Beltran H. The N-myc Oncogene: Maximizing its Targets, Regulation, and Therapeutic Potential. Molecular cancer research : MCR 2014;12(6):815–22.
15. Wachtel M, Schäfer BW. PAX3-FOXO1: Zooming in on an "undruggable" target. Seminars in cancer biology 2018;50:115–23.
16. Carmena M, Earnshaw WC. The cellular geography of aurora kinases. Nature reviews Molecular cell biology 2003;4(11):842–54.
17. Marumoto T, Hirota T, Morisaki T, Kunitoku N, Zhang D, Ichikawa Y, et al. Roles of aurora-A kinase in mitotic entry and G2 checkpoint in mammalian cells. Genes to cells : devoted to molecular & cellular mechanisms 2002;7(11):1173–82.
18. Macůrek L, Lindqvist A, Lim D, Lampson MA, Klompmaker R, Freire R, et al. Polo-like kinase-1 is activated by aurora A to promote checkpoint recovery. Nature 2008;455(7209):119–23.
19. Seki A, Coppinger JA, Jang C-Y, Yates JR, Fang G. Bora and the kinase Aurora a cooperatively activate the kinase Plk1 and control mitotic entry. Science (New York, NY) 2008;320(5883):1655–58.
20. Hannak E, Kirkham M, Hyman AA, Oegema K. Aurora-A kinase is required for centrosome maturation in Caenorhabditis elegans. The Journal of cell biology 2001;155(7):1109–16.
21. Cowley DO, Rivera-Pérez JA, Schliekelman M, He YJ, Oliver TG, Lu L, et al. Aurora-A kinase is essential for bipolar spindle formation and early development. Molecular and cellular biology 2009;29(4):1059–71.
22. Bischoff JR, Anderson L, Zhu Y, Mossie K, Ng L, Souza B, et al. A homologue of Drosophila aurora kinase is oncogenic and amplified in human colorectal cancers. The EMBO journal 1998;17(11):3052–65.
23. Borisa AC, Bhatt HG. A comprehensive review on Aurora kinase: Small molecule inhibitors and clinical trial studies. European journal of medicinal chemistry 2017;140:1–19.
24. Goepfert TM, Adigun YE, Zhong L, Gay J, Medina D, Brinkley WR. Centrosome amplification and overexpression of aurora A are early events in rat mammary carcinogenesis. Cancer research 2002;62(14):4115–22.
25. Zhou H, Kuang J, Zhong L, Kuo WL, Gray JW, Sahin A, et al. Tumour amplified kinase STK15/BTAK induces centrosome amplification, aneuploidy and transformation. Nature genetics 1998;20(2):189–93.
26. Yao J-E, Yan M, Guan Z, Pan C-B, Xia L-P, Li C-X, et al. Aurora-A down-regulates IkappaBalpha via Akt activation and interacts with insulin-like growth factor-1 induced phosphatidylinositol 3-kinase pathway for cancer cell survival. Molecular cancer 2009;8:95.
27. Matsuzaki H, Daitoku H, Hatta M, Aoyama H, Yoshimochi K, Fukamizu A. Acetylation of Foxo1 alters its DNA-binding ability and sensitivity to phosphorylation. Proceedings of the National Academy of Sciences of the United States of America 2005;102(32):11278–83.
28. Ianevski A, He L, Aittokallio T, Tang J. SynergyFinder: a web application for analyzing drug combination dose–response matrix data. Bioinformatics 2017;33(15):2413–15.
29. Abraham J, Nunez-Alvarez Y, Hettmer S, Carrio E, Chen HI, Nishijo K, et al. Lineage of origin in rhabdomyosarcoma informs pharmacological response. Genes Dev 2014;28(14):1578-91.
30. Lee S-Y, Lee GR, Woo D-H, Park NH, Cha HJ, Moon Y-H, et al. Depletion of Aurora A leads to upregulation of FoxO1 to induce cell cycle arrest in hepatocellular carcinoma cells. Cell cycle (Georgetown, Tex) 2013;12(1):67–75.
31. Roux KJ, Kim DI, Raida M, Burke B. A promiscuous biotin ligase fusion protein identifies proximal and interacting proteins in mammalian cells. The Journal of cell biology 2012;196(6):801–10.
32. Kim DI, Jensen SC, Noble KA, Kc B, Roux KH, Motamedchaboki K, et al. An improved smaller biotin ligase for BioID proximity labeling. Molecular biology of the cell 2016;27(8):1188–96.
33. Brockmann M, Poon E, Berry T, Carstensen A, Deubzer HE, Rycak L, et al. Small molecule inhibitors of aurora-a induce proteasomal degradation of N-myc in childhood neuroblastoma. Cancer Cell 2013;24(1):75–89.
34. Marshall AD, Grosveld GC. Alveolar rhabdomyosarcoma - The molecular drivers of PAX3/7-FOXO1-induced tumorigenesis. Skeletal muscle 2012;2(1):25.

35. Mercado GE, Xia SJ, Zhang C, Ahn EH, Gustafson DM, Laé M, et al. Identification of PAX3-FKHR-regulated genes differentially expressed between alveolar and embryonal rhabdomyosarcoma: focus on MYCN as a biologically relevant target. Genes, chromosomes & cancer 2008;47(6):510–20.
36. Richards MW, Burgess SG, Poon E, Carstensen A, Eilers M, Chesler L, et al. Structural basis of N-Myc binding by Aurora-A and its destabilization by kinase inhibitors. Proceedings of the National Academy of Sciences of the United States of America 2016;113(48):13726–31.
37. Welcker M, Orian A, Jin J, Grim JE, Grim JA, Harper JW, et al. The Fbw7 tumor suppressor regulates glycogen synthase kinase 3 phosphorylation-dependent c-Myc protein degradation. Proceedings of the National Academy of Sciences of the United States of America 2004;101(24):9085–90.
38. Chesler L, Schlieve C, Goldenberg DD, Kenney A, Kim G, McMillan A, et al. Inhibition of phosphatidylinositol 3-kinase destabilizes Mycn protein and blocks malignant progression in neuroblastoma. Cancer research 2006;66(16):8139–46.
39. Otto T, Horn S, Brockmann M, Eilers U, Schüttrumpf L, Popov N, et al. Stabilization of N-Myc is a critical function of Aurora A in human neuroblastoma. Cancer Cell 2009;15(1):67–78.
40. Marshall AD, Picchione F, Geltink RI, Grosveld GC. PAX3-FOXO1 induces up-regulation of Noxa sensitizing alveolar rhabdomyosarcoma cells to apoptosis. Neoplasia 2013;15(7):738-48.
41. Cao L, Yu Y, Bilke S, Walker RL, Mayeenuddin LH, Azorsa DO, et al. Genome-wide identification of PAX3-FKHR binding sites in rhabdomyosarcoma reveals candidate target genes important for development and cancer. Cancer Res 2010;70(16):6497-508.
42. Millau J-F, Mai S, Bastien N, Drouin R. p53 functions and cell lines: have we learned the lessons from the past? BioEssays : news and reviews in molecular, cellular and developmental biology 2010;32(5):392–400.
43. Shibue T, Takeda K, Oda E, Tanaka H, Murasawa H, Takaoka A, et al. Integral role of Noxa in p53-mediated apoptotic response. Genes & Development 2003;17(18):2233–38.
44. Guikema JE, Amiot M, Eldering E. Exploiting the pro-apoptotic function of NOXA as a therapeutic modality in cancer. Expert Opin Ther Targets 2017;21(8):767-79.
45. Faqar-Uz-Zaman SF, Heinicke U, Meister MT, Vogler M, Fulda S. BCL-xL-selective BH3 mimetic sensitizes rhabdomyosarcoma cells to chemotherapeutics by activation of the mitochondrial pathway of apoptosis. Cancer Lett 2018;412:131-42.
46. Margue CM, Bernasconi M, Barr FG, Schafer BW. Transcriptional modulation of the anti-apoptotic protein BCL-XL by the paired box transcription factors PAX3 and PAX3/FKHR. Oncogene 2000;19(25):2921-9.
47. Zhao Y, Wang Y, Zhu W-G. Applications of post-translational modifications of FoxO family proteins in biological functions. Journal of molecular cell biology 2011;3(5):276–82.
48. Gierisch ME, Pedot G, Walser F, Lopez-Garcia LA, Jaaks P, Niggli FK, et al. USP19 deubiquitinates EWS-FLI1 to regulate Ewing sarcoma growth. Sci Rep 2019;9(1):951.
49. Bharathy N, Suriyamurthy S, Rao VK, Ow JR, Lim HJ, Chakraborty P, et al. P/CAF mediates PAX3-FOXO1-dependent oncogenesis in alveolar rhabdomyosarcoma. The Journal of pathology 2016;240(3):269–81.
50. Roberts AW, Seymour JF, Brown JR, Wierda WG, Kipps TJ, Khaw SL, et al. Substantial susceptibility of chronic lymphocytic leukemia to BCL2 inhibition: results of a phase I study of navitoclax in patients with relapsed or refractory disease. J Clin Oncol 2012;30(5):488-96.

Figure legends

Figure 1. Silencing of PAX3-FOXO1 induces apoptosis via NOXA

A. Caspase activity after silencing of PAX3-FOXO1. Caspase 3/7 activity was assessed 24, 48 and 72 hours after induction of shRNA expression in Rh4 cells. Mean of three independent experiments; bars, SD; 2-way ANOVA, ***, P ≤ 0.001. B. Western blot analysis of whole cell lysates from Rh4 shsc or shP3F 48h after shRNA induction with doxycycline (+) or no induction (-). C. Z-vad mediated rescue from cell death. WST-1 assay of Rh4 shsc or shP3F treated with doxycycline and increasing concentrations of z-vad FMK. Mean of two independent experiments; bars, SD; Student's *t* test, *, P ≤ 0.05, **, P ≤ 0.01. D. Rescue experiment after shRNA-mediated silencing of PAX3-FOXO1 mRNA. Rh4 cells expressing either scrambled shRNA (shsc) or shRNA targeting PAX3-FOXO1 mRNA (shP3F) were treated for 48h with 0.1 µg/mL doxycycline to induce shRNA expression. Viability was assessed using WST-1 assay and shown relative to non-treated cells. Several cell death inhibitors were used at the concentration indicated. Mean of two independent experiments; bars, SD. E. BH-3 only protein screen. Caspase 3/7 activity of Rh4 shP3F cells harboring CRISPR/Cas9-induced knockouts of the indicated genes (sc = scrambled sgRNA). White bars, no shRNA induction; black bars, 48h after doxycycline-induced shRNA expression. Mean of two independent experiments; bars, SD. F. NOXA expression after PAX3-FOXO1 silencing. Western blot analysis of whole cell lysates from Rh4 shsc or shP3F 48h after shRNA induction with doxycycline (+) or no induction (-). G. Relative mRNA expression of the PMAIP1 gene in Rh4 shsc or shP3F 48h after induction of shRNA with doxycycline. Gene expression was normalized to GAPDH. Mean of two independent experiments. Each experiment was performed in triplicates.

Figure 2. Navitoclax sensitizes cells to cell death after silencing of PAX3-FOXO1

A. Drug screen to enhance cell death after silencing of PAX3-FOXO1. Rh4 shsc and Rh4 shP3F cells were treated with drugs (Supplemental Table 1) while simultaneously inducing shRNA expression with 0.1 µg/mL doxycycline for 48h. Viability was measured by WST-1 assay and the relative viability effect

of each drug was calculated (see Method section). Left Panel: Plot shows the mean viability from 3 independent experiments performed in duplicates. Right Panel: List of the top hits according to the ratio of relative viability of drugs on shP3F over shsc. Ranked according to their targeting class. SD = standard deviation; Welch's two-tailed t-test, *, P ≤ 0.05, **, P ≤ 0.01, ***, P ≤ 0.001. B. Individual effect of Navitoclax on relative cell viability of Rh4 shsc or Rh4 shP3F compared to DMSO; SD; Welch's two-tailed t-test, **, P ≤ 0.01. C-E. Relative cell viability of Rh4 shsc or Rh4 shP3F cells after 48h with or without shRNA induction and simultaneous treatment with increasing concentrations of navitoclax, venetoclax or A-1331852, respectively. Mean +/- SD from three independent experiments performed in triplicates. IC_{50} values were calculated from non-linear regression analysis using GraphPad Prism® 7. F. Relative cell viability of Rh4 shsc *PMAIP*$^{-/-}$ or Rh4 shP3F *PMAIP*$^{-/-}$ cells treated with increasing concentrations of navitoclax for 48h.

Figure 3. Inhibition of Aurora Kinase A leads to reduced PAX3-FOXO1 protein stability

A. PAX3-FOXO1 protein levels were assessed by Western Blot 48h after treatment with 100 nmol/L of compounds (Supplemental table 1). Protein bands were analyzed by densitometry and normalized to GAPDH levels. Treatment was compared to DMSO. B. Exemplary blot of one set of drugs. Aurora Kinase A inhibitors are labelled in red. C: Chart showing the classes of inhibitors found among the top candidates. Red: Aurora Kinase A inhibitors, green: CDK9 inhibitors, grey: epigenetic modulators. D. Western Blot of lysates from Rh4 cells treated for 48h with increasing concentrations of the given drug. Left panel: Alisertib, right panel: AT9283. E. Immunoblot for phosphorylation at the indicated sites. Cells were incubated for 24h with alisertib and lysed with Co-IP buffer. F. Western Blot of RD cells transiently transfected with the respective overexpression plasmid for PAX3-FOXO1 mutants or wild-type (wt). 8h before lysis cells were treated with either 10 µg/mL cycloheximide (CHX) or DMSO to block protein synthesis. G. Densitometric quantification of the fusion protein levels, normalized to GAPDH. Mean of three independent experiments; bars, SD; two-way ANOVA, *, P < 0.05, **, P < 0.01. H. Western Blot analysis of streptavidin pull-down experiments. HEK293T cells were transduced with a PAX3-FOXO1 expression plasmid fused to BirA biotin ligase (P3F-BirA) or with GFP or BirA alone. Cells were incubated with biotin (+) or not (-) and lysed. Pull-down was performed with beads coated with streptavidin.

Figure 4. Aurora kinase A regulates MYCN in rhabdomyosarcoma cells and affects MYCN protein stability.

A. RMS cell lines were transduced with lentivirus containing control or Aurora kinase A (AURKA) shRNA (B and C) plasmids. Following selection, cells were lysed and immunoblotted for MYCN. MYCN was reduced in AURKA silenced cells in comparison to control shRNA treated cells. B. AURKA shRNA and control treated cells were transfected with V5-tagged MYCN (either wild-type (WT) or T58A/S62A mutant (MT) plasmid), lysed after 48 hours and immunoblotted with V5 antibody. V5-MYCN (wild type) was reduced in AURKA silenced cells compared to controls however V5-MYCN (mutant) was not, indicating that AURKA can regulate MYCN post-translationally in rhabdomyosarcoma cells by affecting protein stability. C. RMS-01 and RH4 were treated with increasing doses of alisertib and lysed after 48 hours to assess MYCN and PAX3-FOXO1 protein levels by immunoblot.

Figure 5. Navitoclax and alisertib synergistically induce cell death in vitro

A. Synergy screen. Rh4 cells were incubated with each drug (Supplemental Table 1) at a concentration of 500 nmol/L and additionally with either 800 nmol/L Navitoclax or DMSO. After 48h viability was assessed by WST-1 assay. Left y-axis: black bars, compound; grey bars, compound plus Navitoclax. Right y-axis, red bars: viability ratio (+Navitoclax/+DMSO). Top hits with a viability ratio < 0.7 are shown and ranked according to viability of each drug alone. Red stars: Aurora Kinase A inhibitors. Circle plot: 28 top hits were classified according to their target spectrum: red, Aurora Kinase A inhibitors. B. Relative cell viability in percent after cross-titration of alisertib against Navitoclax in Rh4 cells. Cell viability relative to DMSO control was measured after 48h. Color scheme: high viability, blue; low viability: red. Mean values of three independent experiments performed in duplicates is depicted. C. BLISS synergy scores of Rh4 cells, indicated 6 PDX-derived primary cell cultures, human foreskin fibroblasts (HFF) and human myoblasts. Synergy was calculated according to the Bliss independence model using the SynergyFinder WebApp (28). Positive values (red) indicate synergy, negative values (green) indicate antagonism. E. Cell cycle analysis of Rh4 cells treated with given concentrations of Alisertib and additionally with either DMSO or 800 nmol/L Navitoclax. After 24h cells were stained with propidium iodide (PI) and cell cycle was analyzed by flow cytometry. Mean of two independent experiments.

Figure 6. Combination of Navitoclax and alisertib reduces tumor growth in vivo

Rh4 or IC_pPDX35 cells were injected s.c. into the flanks of NSG mice. After engraftment, mice were randomized and assigned into one of four treatment groups: Vehicle (black), Navitoclax only (grey, 3d / week 80 mg/kg), Alisertib only (beige, 5d / week 30 mg/kg), Navitoclax + Alisertib combination (red). Mice were treated for 3 weeks with the respective regimen through administration p.o. (see also Suppl.Fig.7A) and sacrificed when tumors reached a size of 1000 mm^3.

A. Tumor growth of Rh4 cells in vivo. Black arrow: start of treatment. Red box indicates treatment period. Per group: n = 6; error bars, S.E.M. B. Kaplan-Meier graph showing percent survival of different treatment groups. Mantel-Cox test for comparison of survival curves, ***, p = 0.001 C. Tumor growth of IC_pPDX35 tumors. Black arrow: start of treatment. Red box indicates treatment period. Per group: n = 5; error bars, S.E.M. D. Kaplan-Meier graph showing percent survival. E. Histology of engrafted IC_pPDX35 tumors after one week of treatment with either vehicle control (left panel) or combination of Navitoclax (80 mg/kg) and Alisertib (30 mg/kg) (right panel). N = 3. Upper panel: Hematoxylin & Eosin (HE) staining. Bars = 20 µm. Black arrows: apoptotic cells, red arrow: mitotic cell. Lower panel: Immunohistochemical staining against cleaved caspase 3. Bars = 50 µm. Representative images of sections from 3 different mice per group.

Figure 1

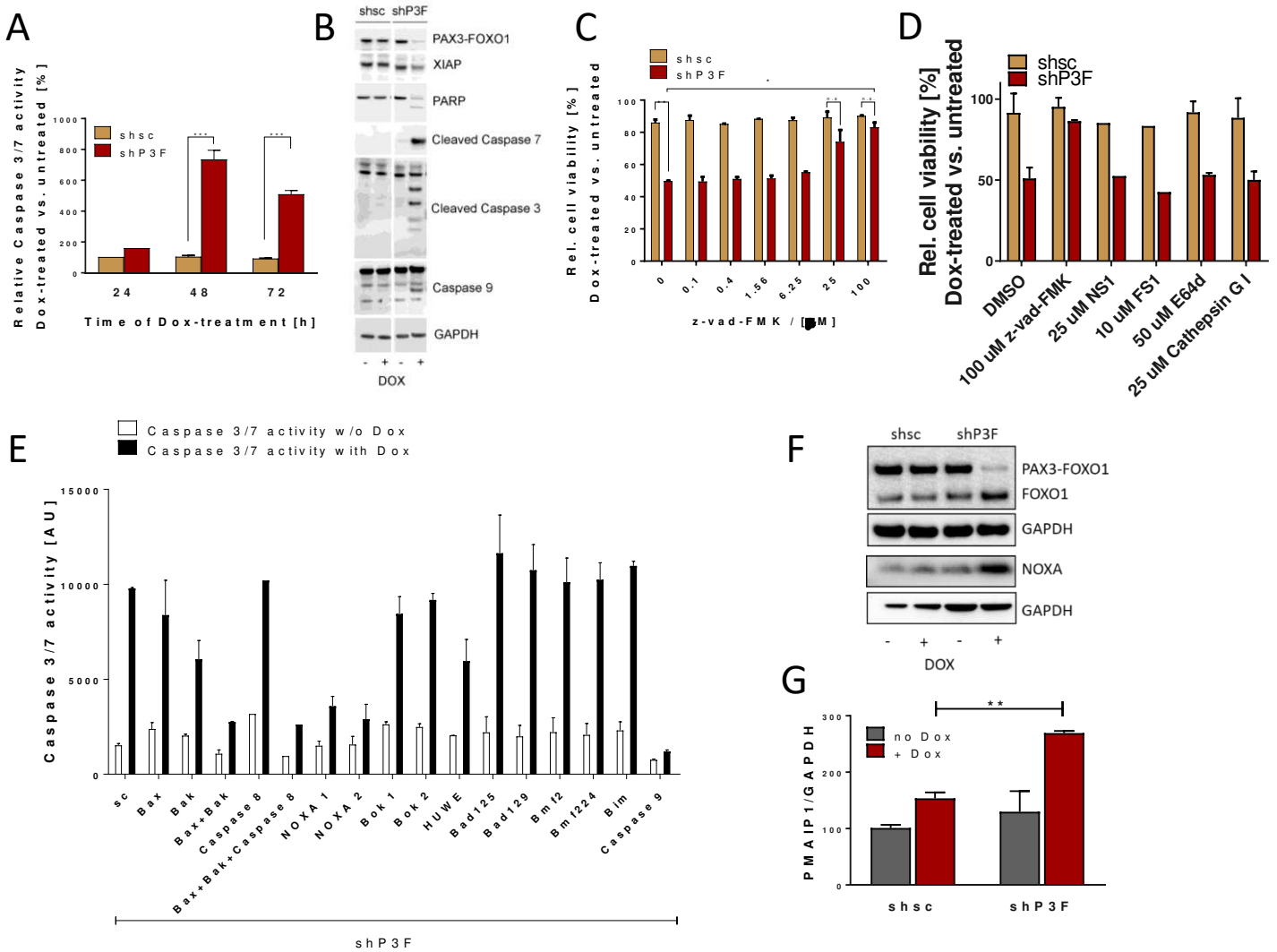

Figure 2

A

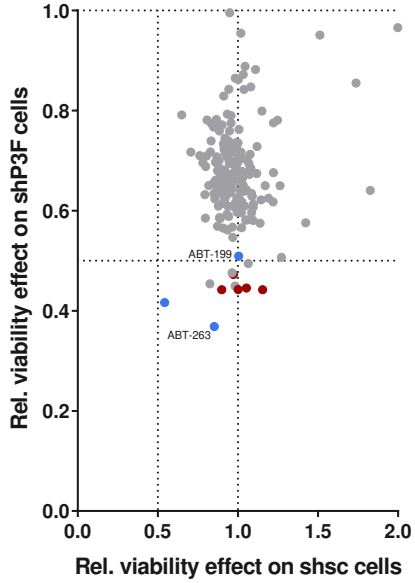

Name	Class	Mean viability effect	SD	Mean viability effect	SD	p-value
		Rh4 shsc		Rh4 shP3F		
ABT-263	BH3-mimetic	0.852	0.0606	0.369	0.0799	**
Obatoclax		0.543	0.3474	0.416	0.2277	n.s.
ABT199		1.005	0.0142	0.509	0.0144	**
AT9283	Aurora Kinase A inhibitor	0.899	0.0632	0.442	0.0527	**
Danusertib		1.154	0.2453	0.442	0.0812	*
Tozasertib		1.001	0.1441	0.442	0.0754	*
Alisertib		1.053	0.1868	0.445	0.0623	*
AMG-900		0.972	0.0968	0.473	0.0639	**
Rigosertib	PLK1 inhibitor	0.982	0.0531	0.45	0.2448	n.s.
Dasatinib	Bcr-Abl inhibitor	0.826	0.0221	0.454	0.0271	***
Ispinesib	KSP inhibitor	0.964	0.0785	0.476	0.1778	*
OTX015	Bromodomain inh	1.065	0.2235	0.494	0.0405	*
AZD7762	Chk1 inhibitor	1.271	0.1816	0.507	0.2735	**

B

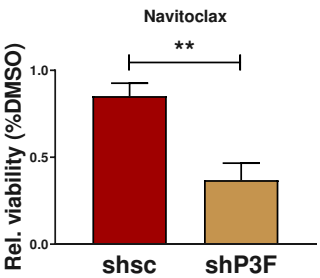

C Navitoclax

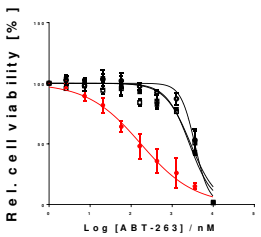

IC50 = 2.6 – 3.5 µM
IC50 = 0.18 µM

D ABT-199

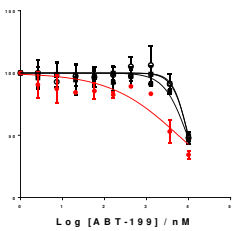

IC50 = 9.2 – 10 µM
IC50 = 5.6 µM

E A-1331852

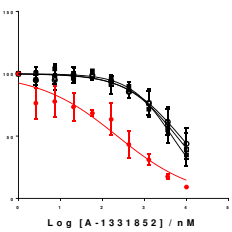

IC50 = 4.5 – 7.0 µM
IC50 = 0.23 µM

F Navitoclax

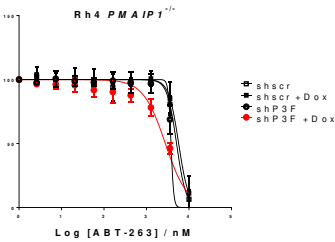

Figure 3

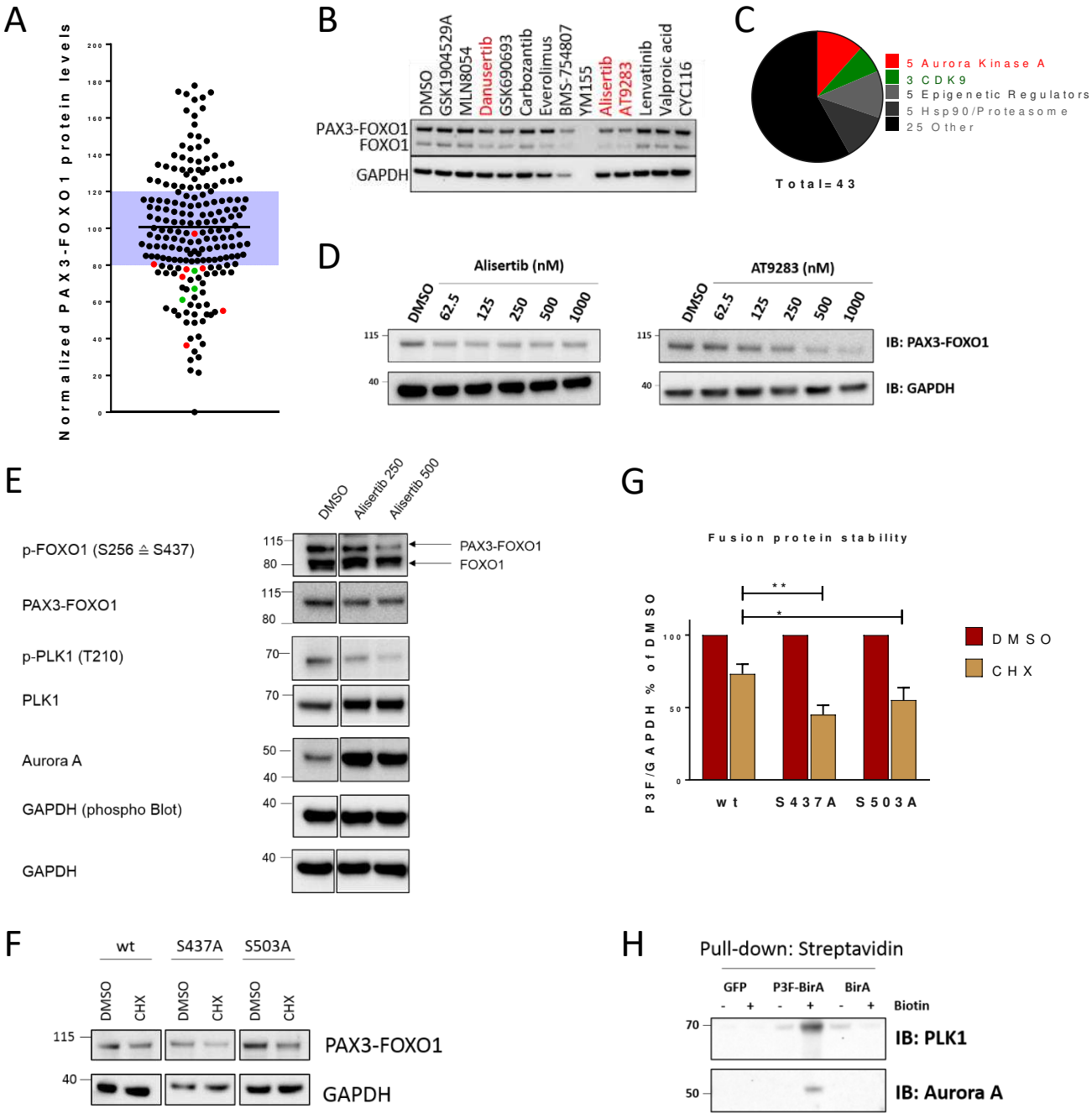

Figure 4

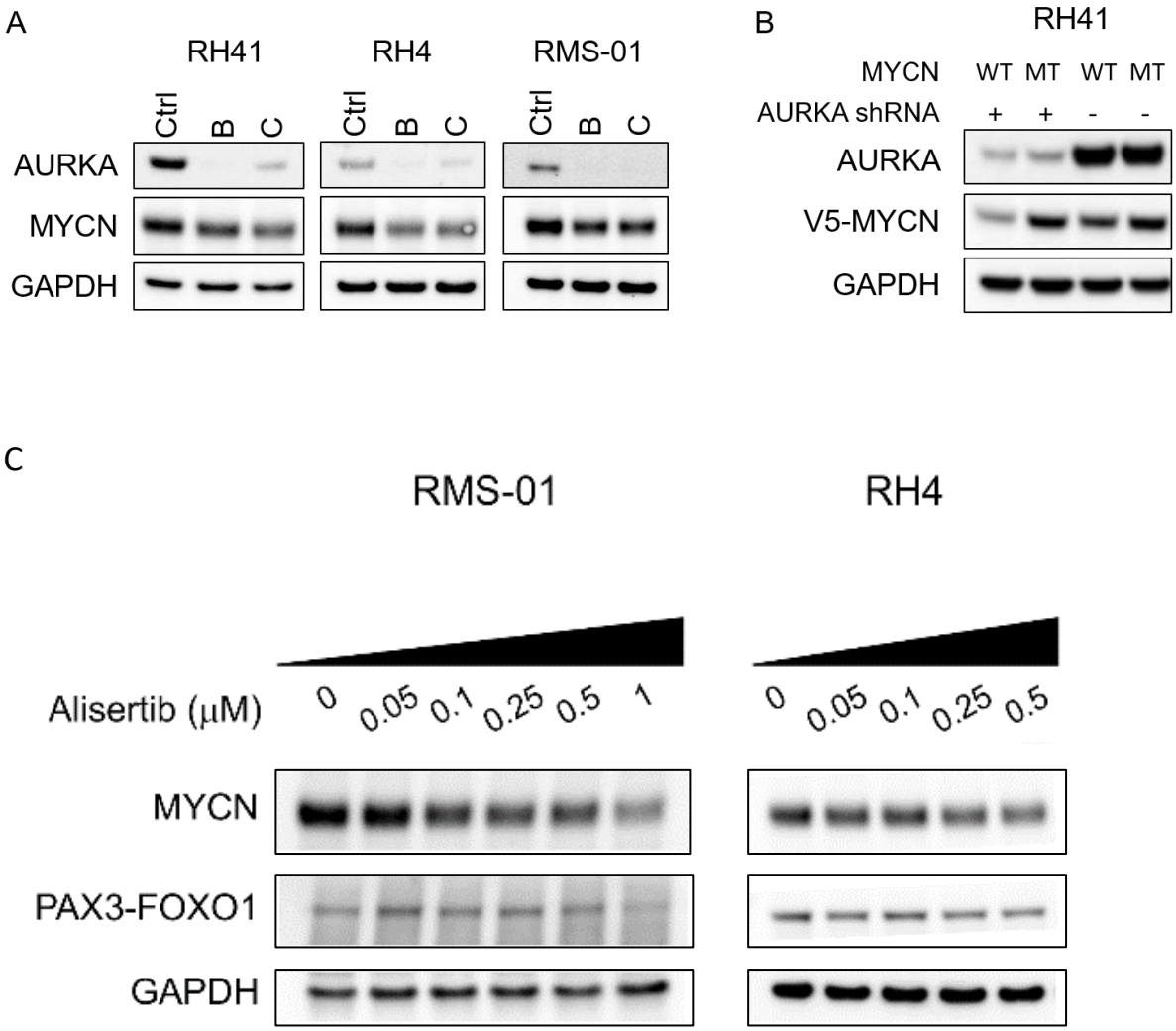

Figure 5

A

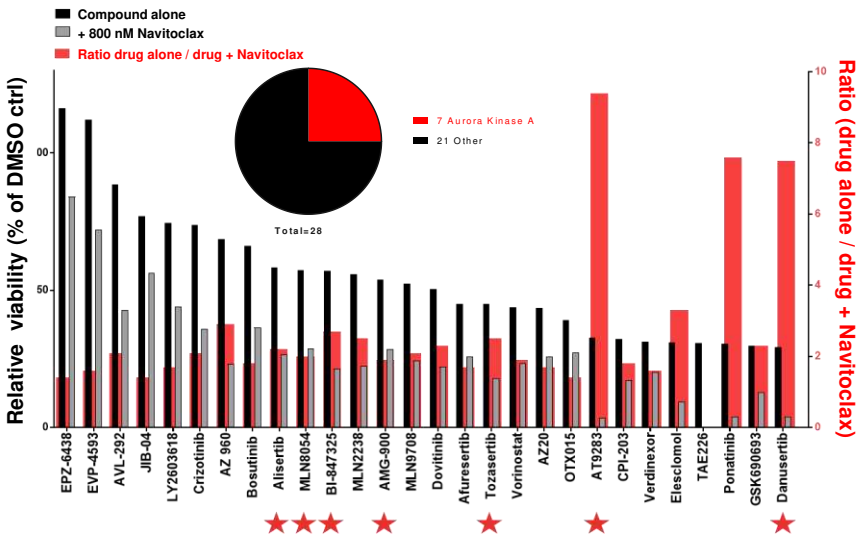

B

Rh4

[ABT263] / nM \ [ALISERTIB] / nM	0	7	16	41	102	255	638	1597	3966	10000
0	100	94	97	79	72	74	70	67	61	50
7	95	97	95	79	71	69	66	67	59	48
16	95	91	86	73	64	63	56	58	56	46
41	94	92	88	70	64	60	59	58	50	41
102	86	86	79	60	46	51	46	43	41	33
255	86	88	80	56	47	42	41	40	35	31
638	74	75	67	46	35	37	34	35	26	23
1597	69	72	63	41	33	34	32	32	23	16
3996	64	61	54	31	21	26	24	23	20	15
10000	21	18	16	11	9.1	9.5	9.3	9.3	5.9	1.4

C

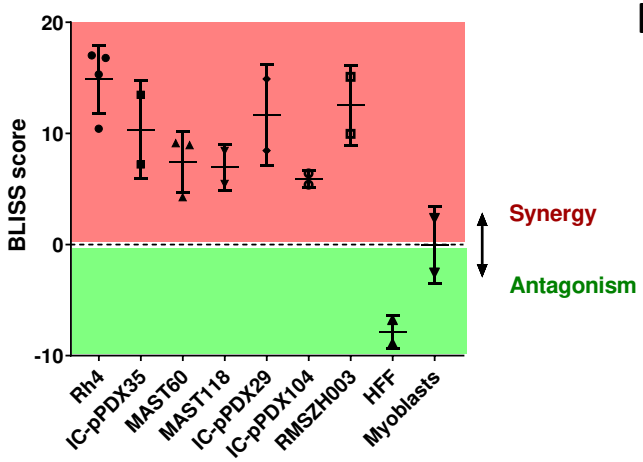

D

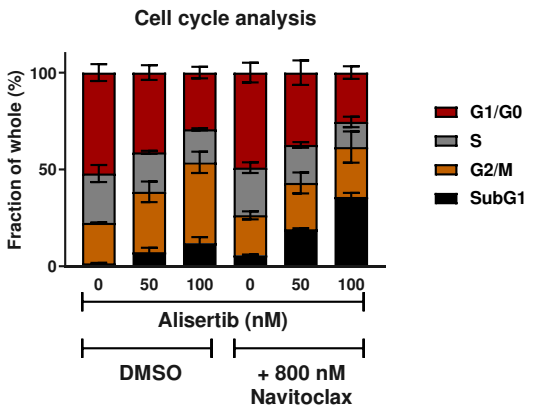

Figure 6

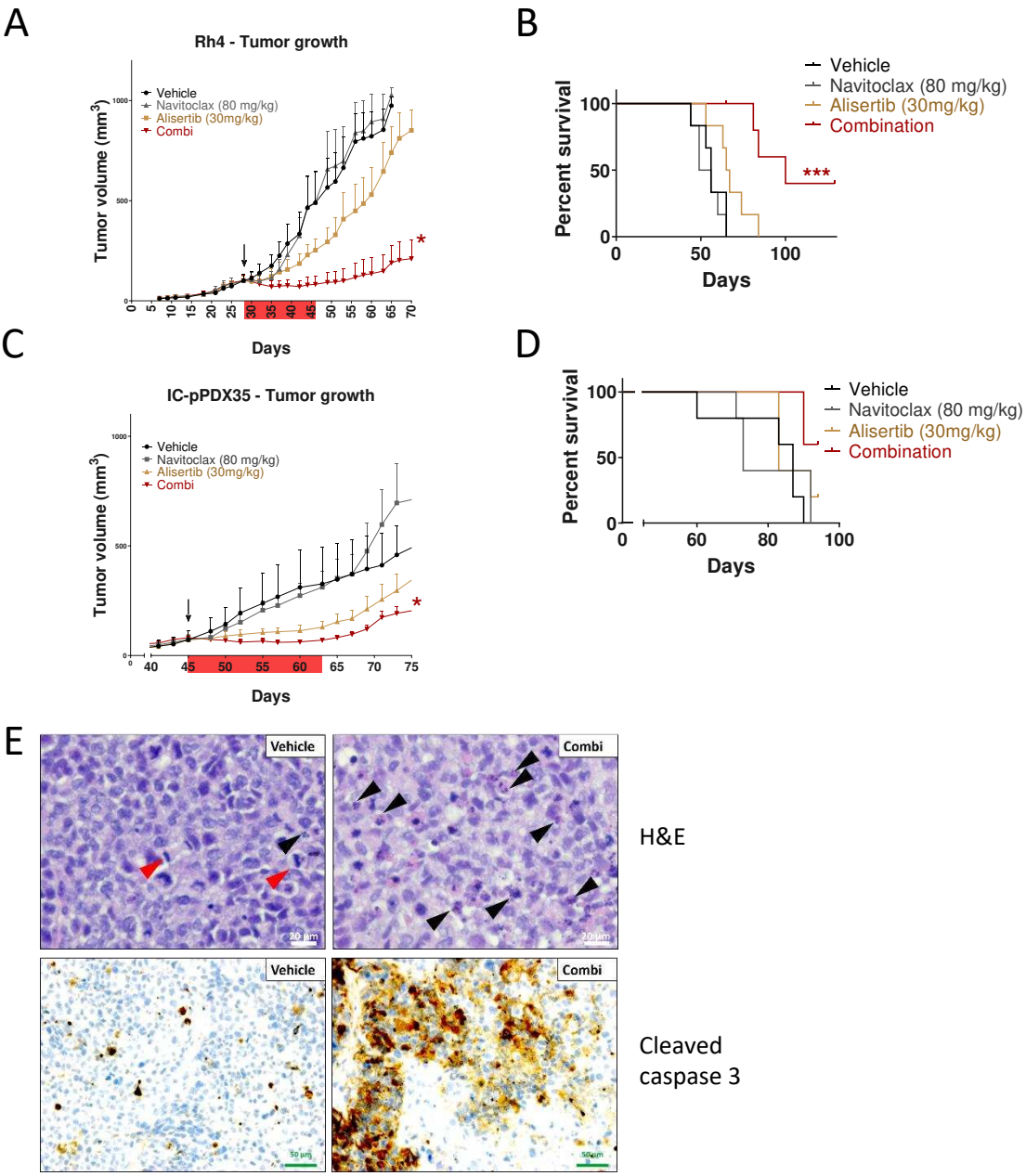

AACR American Association for Cancer Research

Cancer Research

The Journal of Cancer Research (1916–1930) | The American Journal of Cancer (1931–1940)

Aurora A kinase inhibition destabilizes PAX3-FOXO1 and MYCN and synergizes with Navitoclax to induce Rhabdomyosarcoma cell death

Johannes Ommer, Joanna L Selfe, Marco Wachtel, et al.

Cancer Res Published OnlineFirst December 30, 2019.